Chinese Chemical Letters 33 (2022) 4659–4663

Contents lists available at ScienceDirect

Chinese Chemical Letters

journal homepage: www.elsevier.com/locate/cclet

Effects of subtle change in side chains on the photovoltaic performance of small molecular donors for solar cells

Xiang Gao[a,1,*], Kuibao Yu[b,1], Yanjiao Zhao[a,1], Tao Zhang[a], Jing Wen[a], Zifeng Liu[a], Zhihao Liu[a], Guofeng Ye[a], Jianhong Gao[a], Ziyi Ge[b,c,**], Zhitian Liu[a,*]

[a] Hubei Engineering Technology Research Center of Optoelectronic and New Energy Materials, Hubei Key Laboratory of Plasma Chemistry and Advanced Materials, School of Materials Science and Engineering, Wuhan Institute of Technology, Wuhan 430205, China
[b] Ningbo Institute of Materials Technology and Engineering, Chinese Academy of Sciences, Ningbo 315201, China
[c] Center of Materials Science and Optoelectronics Engineering, University of Chinese Academy of Sciences, Beijing 100049, China

ARTICLE INFO

Article history:
Received 16 November 2021
Revised 12 December 2021
Accepted 22 December 2021
Available online 26 December 2021

Keywords:
Organic solar cells
Small molecular donor materials
Chlorination
Miscibility
Photovoltaic performance

ABSTRACT

Small-molecule organic solar cells (SMOSCs) have attracted considerable attention owing to the merits of small molecules, such as easy purification, well-defined chemical structure. To achieve high-performance SMOSCs, the rational design of well-matched donor and acceptor materials is extremely essential. In this work, two new small molecular donor materials with subtle change in the conjugated side thiophene rings are synthesized. The subtle change significantly affects the photovoltaic performance of molecular donors. Compared with chlorinated molecule MDJ-Cl, the non-chlorinated analogue MDJ exhibits decreased miscibility with the non-fullerene acceptor Y6, can more efficiently quench the excitons of Y6. As a result, a improved PCE of 11.16% is obtained for MDJ:Y6 based SMOSCs. The results highlight the importance of fine-tuning the molecular structure to achieve high-performance SMOSCs.

Bulk heterojunction (BHJ) organic solar cells (OSCs) have exhibited the advantages of lightweight, large-area fabrication and flexibility comparison with inorganic solar cells [1–8]. The active layer of organic solar cells plays a crucial role in improving device performance. Divided by photovoltaic components, OSCs can be classified as polymer solar cells (PSCs) which contains polymer donor material and molecular electron acceptors, all-polymer solar cells (all-PSCs), and small-molecule organic solar cells (SMOSCs). SMOSCs have the advantages of easy purification, well-defined chemical structures. Theoretically, SMOSCs are free of batch-to-batch variation which is vital for scale production [9–12]. However, the power conversion efficiencies (PCEs) of SMOSCs lag far behind PSCs. SMOSCs cannot form strong enough intermolecular entanglement and intermolecular interaction due to the limited conjugation length [13–15]. In addition, the inferior PCEs of SMOSCs are caused by low short-circuit current density (J_{sc}) and fill factor (FF), which are mainly attributed to the unfavorable BHJ morphology, resulting in inadequate exciton dissociation and serious charge recombination [16,17].

In recent years, molecular engineering for the construction of A-D-A type small molecule donor has received a lot of attention [18–22]. A-D-A type small molecule donor consists of an electron donating (D) unit as the central moiety and two electron accepting (A) units as the end group. Undoubtedly, the photovoltaic performance could be improved via tuning the backbone structure. For example, Zhou *et al.* designed a highly crystalline small-molecule donor, ZR1, by replacing the conventional trithiophene with electron-rich dithieno[2,3-*d*:2′,3′-*d*′]benzo[1,2-*b*:4,5-*b*′]dithiophene (DTBDT) as the donor D unit, The DTBDT unit effectively extended the conjugation plane and improved the molecular planarity, thus, the optimized ZR1:Y6 based devices reached best PCE of 14.34% (certified PCE of 14.1%) and exhibited a low E_{loss} of 0.52 eV [23].

On the other hand, organic small molecule properties are extremely sensitive to small changes in chemical structure, such as introducing heteroatoms or subtle change in side chain, which modulate not only the crystallinity but also the compatibility of the donor and acceptor [24–26]. For example, Ge *et al.* designed and synthesized a novel small molecular donor of BT-2F based on previously reported BTEC-2F [27]. The shortened alkyl-chains with higher regularity endow BT-2F with more ordered packing arrange-

* Corresponding authors.
** Corresponding author at: Ningbo Institute of Materials Technology and Engineering, Chinese Academy of Sciences, Ningbo 315201, China.
E-mail addresses: xgao@wit.edu.cn (X. Gao), geziyi@nimte.ac.cn (Z. Ge), able.ztliu@wit.edu.cn (Z. Liu).
[1] These authors contributed equally to this work.

https://doi.org/10.1016/j.cclet.2021.12.055
1001-8417/

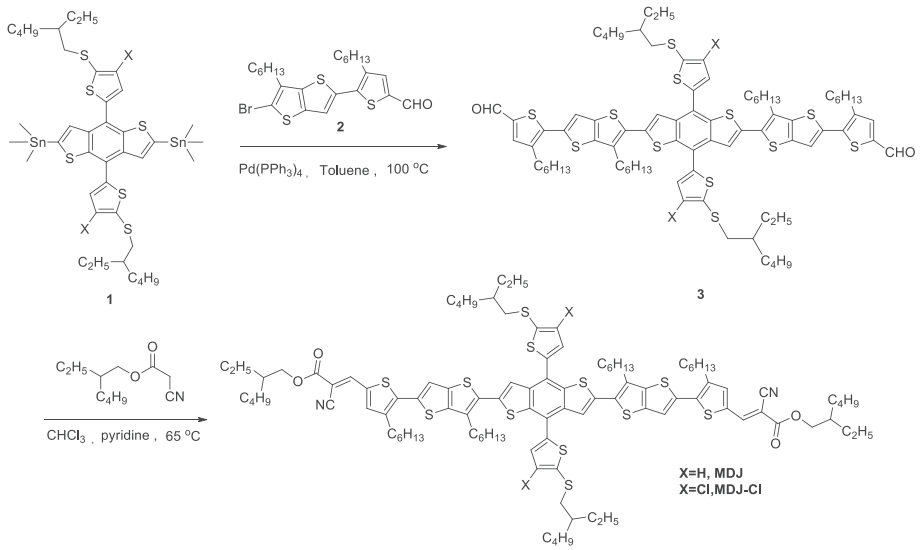

Fig. 1. Synthetic routes for MDJ and MDJ-Cl.

ment and more compact lamellar stacking. By blending with Y6 or N3, BT-2F based devices showed impressive PCEs of 13.80% and 14.09% respectively. Chen et al. used a Cl atom to replace a pair of alkyl chains of BTR to synthesize BTR-Cl. Thus, the BTR-Cl exhibited higher crystallinity and lower highest occupied molecular orbital (HOMO) level than BTR. Finally, BTR-Cl:Y6-based device produced an improved PCE of 13.61% [28]. Zhou et al. synthesized the materials ZR2-C1, ZR2-C2, ZR2-C3 by altering the side-chain branching position of thiophene. With the side-chain branching position moving away from core moiety, the π-π stacking interactions of the molecules are increased. ZR2-C3 achieved the highest PCE of 14.3% among these three molecules [29]. Hou *et al.* synthesized material B1 by using the symmetric phenyl units as the side group of the central backbone, which improved the stability of the molecular conformation and greatly enhanced the crystallinity. A PCE of 15.3% was obtained by pairing B1 with BO-4Cl [30]. Similar results could be obtained by introduction of fluorine, or bromine atoms into specific positions of some representative units. Li *et al.* synthesized two new small molecule donors, including SM1-S with alkylthio and SM1-F with fluorine and alkyl substituents. The SM1-F-based SMOSCs demonstrated better PCE of 14.07% with a preferable FF of 0.699 and a higher V_{oc} of 0.866 V [31].

Based on the consideration mentioned above, we have designed and synthesized two small-molecule donors consisting with chlorinated and/or alkylthio substitutions, MDJ-Cl and MDJ respectively. Two-dimension electron-rich benzodithiophene (BDT) was selected as the donor core because of its excellent charge transfer properties, the 2-ethyl hexyl cyanoacetate was used as the end group to lower down the energy levels and broaden the absorption, and the thieno[3,2-*b*]thiophene was chose as the link bridge because of the straight line skeleton and the fused rings can facilitate the π–π stacking and intermolecular charge transportation [32–35]. When the small donors were blended with Y6, the MDJ-Cl:Y6-based device gave a moderate PCE of 4.96%, while the MDJ:Y6-based device showed an impressive PCE of 11.16%. The different PCEs of these two SM donors were carefully analyzed by studying the intrinsic properties of the two donors, the BHJ morphology and photophysical process in SMOSC.

The synthetic route of the molecules MDJ-Cl and MDJ are illustrated in Fig. 1, and the detailed synthesis process can be seen in Supporting information. Small molecule donors, MDJ and MDJ-Cl were synthesized by Stille coupling and Knoevenagel condensation in sequence. The molecular structures of MDJ and MDJ-Cl are confirmed by ^{1}H NMR, ^{13}C NMR and mass spectra. Both MDJ and MDJ-Cl display an excellent solubility in common solvents such as dichloromethane, chloroform, chlorobenzene, tetrahydrofuran and toluene due to the multiple alkyl chains. Thermal gravimetric analysis (TGA) indicates that the two materials have good thermal stabilities with 5% weight loss decomposition temperatures of 359.8 °C for MDJ-Cl and 354.6 °C for MDJ, respectively (Fig. S8 in Supporting information).

Both small molecule donors exhibit similar absorption peaks in solution and film. In the solution, the two small donor molecules show strong absorption bands in the range of 300–590 nm as shown in Fig. 2a, and the maximum molar extinction coefficients were calculated to be 9.02×10^4 and 7.65×10^4 L mol^{-1} cm^{-1} for MDJ-Cl and MDJ, respectively (Fig. S9 in Supporting information). In the film state, the spectrum of MDJ presents an absorption peak at 550 nm and a strong absorption in the entire visible light region (300–700 nm). Compared with MDJ, MDJ-Cl exhibits a slight blue-shifted absorption peak (8 nm) in both solution and films, which could be attributed to the electron withdrawing ability of chlorine atoms leading to a reduction in the electron density of the donor unit, thus hindering the intramolecular charge transfer along the backbone [36]. The distinguished shoulder peaks of MDJ and MDJ-Cl which located at 664 nm and 656 nm, respectively, indicate the accumulation of molecular backbones and strong intermolecular interactions. However, MDJ-Cl shows stronger shoulder peaks than MDJ, indicating a stronger preaggregation [37]. Both molecules exhibit the complementary absorption spectrum matched with the star molecular acceptor Y6, which is conducive to fabricate efficient non-fullerene OSCs with high short-circuit current density (J_{sc}) [38].

The energy levels of molecules are measured by square wave voltammogram (SWV) according to the oxidation and reduction onset potential. The HOMO and lowest unoccupied molecular orbital (LUMO) energy levels of MDJ are −5.36 eV and −3.59 eV (Fig. 2b). The HOMO/LUMO energy levels of MDJ-Cl turned out to be lower (−5.53/−3.59 eV) because of chlorination. The deeper HOMO energy level of MDJ-Cl and the proper energy level alignment with Y6 (−5.71/−4.10 eV) [39] make it possible to achieve high open circuit voltage (V_{oc}). In addition, both MDJ and MDJ-Cl exhibit homogeneous and well delocalized electron distribution along the main chain as shown in Figs. 2c and d and the calculated HOMO/LUMO

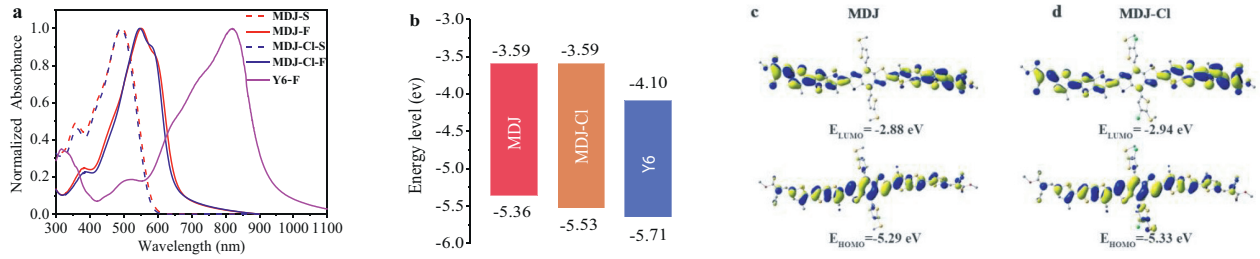

Fig. 2. (a) Normalized absorption spectra of MDJ, MDJ-Cl and Y6 in the $CHCl_3$ solution and thin film. (b) Energy level diagram of materials used in the device. Electron density distributions of LUMO and HOMO for (c) MDJ and (d) MDJ-Cl.

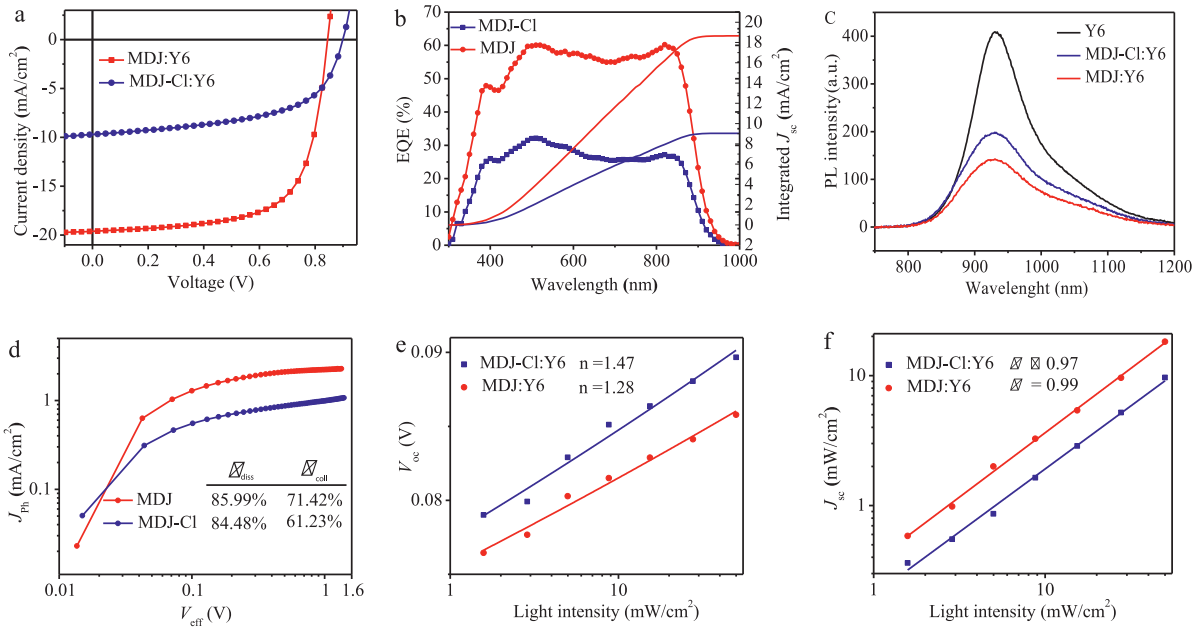

Fig. 3. (a) The *J-V* curves and (b) EQE curves of the champion solar cells based on MDJ:Y6. MDJ-Cl:Y6 prepared under the optimal conditions. (c) Photoluminescence spectra of the Y6 neat film and the blend film (MDJ:Y6; MDJ-Cl:Y6) excited at 639 nm. (d) Photocurrent density (J_{ph}) *versus* effective voltage (V_{eff}) curves of the devices. (e) V_{oc}-light intensity and (f) J_{sc}-light intensity relationships.

Table 1
Photovoltaic properties of nonfullerene all-small-molecule solar cells.

Active layer	V_{oc} (V)	J_{sc} (mA/cm^2)	J_{calcd}.[a] (mA/cm^2)	FF (%)	PCE (ave.[b]) (%)	Hole mobility (μ_h) (cm^2 V^{-1} s^{-1})	Electron mobility (μ_e) (cm^2 V^{-1} s^{-1})
MDJ:Y6	0.844	19.59	18.65	67.42	11.16 (11.02)	1.76×10^{-4}	4.37×10^{-4}
MDJ-Cl:Y6	0.896	9.69	9.05	57.12	4.96 (4.81)	0.46×10^{-4}	2.79×10^{-4}

[a] Values calculated from EQE.
[b] The average values of the device parameters.

levels for MDJ and MDJ-Cl are −5.29/−2.88 eV and −5.33/−2.94 eV, respectively.

In order to investigate the photovoltaic performance of the two donor materials, OSCs with a traditional device structure of ITO/PEDOT:PSS/small molecular donor: Y6/PDINO/Al were fabricated. The detailed process of device preparation is described in the supporting information. The optimized device used chloroform as the solvent, and were heat-annealed at 100 °C for 10 min. The weight ratio of D/A was 1.5:1, with a total concentration of 20 mg/mL. The current-voltage curves of the optimal OSCs are showed in Fig. 3a, and Table 1 shows the corresponding photovoltaic parameters. The device based on MDJ-Cl revealed a V_{oc} of 0.896 V, a J_{sc} of 9.69 mA/cm^2, an FF of 57.12% and ultimately a modest PCE of 4.96%. In contrast, the MDJ based device showed an excellent PCE of 11.16% with a V_{oc} of 0.844 V, a significantly increased J_{sc} of 19.59 mA/cm^2 and an FF of 67.42%. The different V_{oc} values of the two devices can be attributed to their HOMO levels. Fig. 3b shows the external quantum efficiency (EQE) curves of the best MDJ/Y6 and MDJ-Cl/Y6 co-blended films. The MDJ/Y6 blend covers a broader and stronger photoresponse range from 300 nm to 935 nm. The maximum EQE of the best MDJ/Y6 blended film is 60% at 500 nm, which is 1.9 times higher than that of the optimal MDJ-Cl/Y6 blended film. This agrees with the higher J_{sc} values of MDJ/Y6 blends. By integrating the EQE data, the J_{sc} values for the MDJ and MDJ-Cl based OSCs were calculated to be 18.65 mA/cm^2 and 9.05 mA/cm^2, respectively. The integral J_{sc} values calculated from the EQE curves matched well with the J_{sc} values obtained from the *J-V* curves (error <5%).

Because the LUMO energy offset between the donor molecules and Y6 is as large as 0.5 eV, which is believed large enough for exciton dissociation [40]. Given the fact that chlorination lowered the HOMO energy of MDJ-Cl, the photoluminescence (PL) spectra of Y6

and their blend films were recorded (Fig. 3c) with excitation at 639 nm, to explore the dissociation of the photo-induced excitons of Y6 and hole transfer behavior from Y6 to molecular donors. The photoluminescence of pristine Y6 exhibits a broad emission with a peak at 931 nm. When blending donor and accepter together, the PL intensities of Y6 are greatly quenched, indicating that the excitons of Y6 could be efficiently dissociated in both blends. However, the maximum fluorescence intensity of the blend film of MDJ:Y6 is obviously lower than that of MDJ-Cl:Y6, which indicates that the excitons of Y6 dissociated more efficiently in the blend of MDJ:Y6, which would further contribute to the enhanced EQE and J_{sc} values.

The relationship between the photocurrent density (J_{ph}) and the effective voltage (V_{eff}) provides more information about exciton dissociation and charge collection in the active layer. J_{ph} is defined as the difference between the photocurrent density (J_L) and the dark current density (J_D), and V_{eff} is defined as the difference between the compensating voltage (V_0, depends on $J_{ph} = 0$) and the applied voltage (V) [41,42]. At low values of V_{eff}, the photocurrent increases linearly with voltage. J_{ph} saturates when the effective voltage is large enough to dissociate all photo-generated excitons, defined as the saturation photocurrent density (J_{sat}). The exciton dissociation efficiency (η_{diss}) and charge collection efficiency (η_{coll}) can be calculated from ${J_{ph}}^a/J_{sat}$ and ${J_{ph}}^b/J_{sat}$. ${J_{ph}}^a$ and ${J_{ph}}^b$ are J_{ph} under short circuit and maximum power output conditions, respectively. As shown in Fig. 3d, under short-circuit conditions, the η_{diss} were calculated to be 85.99% for the MDJ:Y6 blend and 84.48% for the MDJ-Cl:Y6 blend; η_{coll} were calculated to be 71.42% for the MDJ:Y6 blend and 61.23% for the MDJ-Cl:Y6 blend under maximum power conditions. MDJ:Y6 exhibited a higher exciton dissociation and charge collection efficiency, ensuring a higher FF of 67.42% and J_{sc} of 19.59 mA/cm^2.

In addition, device performance is closely related to the charge-carrier recombination process in OSCs. We investigated the light intensity dependence of V_{oc} and J_{sc} in the devices to assess the charge recombination process, and the corresponding results are shown in Fig. 3e. The relationship of V_{oc} and corresponding incident light intensity (P_{light}) can be fitted by the equation $V_{oc} \propto nkT/q \ln(P_{light})$, where k is the Boltzmann constant, T is the temperature in Kelvin, and q is the elementary charge. The parameter n indicates the extent to which the BHJ suffers from trap-induced recombination. Typically, n varies between 1 and 2; the larger the deviation from 1, the severer trap-assisted recombination. The slope for the MDJ:Y6 device is 1.28 kBT/q, which is smaller than that of MDJ-Cl:Y6 device (1.47 kBT/q). This result suggests that bimolecular recombination dominates in both SMOSCs and less trap-assisted recombination in the MDJ:Y6 device. In addition, the relationship between J_{sc} and P_{light} can be described as a power-law dependence equation for $J_{sc} \propto {P_{light}}^{\alpha}$, where α represents the extent of bimolecular recombination in the BHJ OSCs [43,44]. If more dissociated free charge carriers can be swept out and collected by the electrodes prior to recombination, α is closer to 1 ($\alpha \leq 1$). By fitting the double logarithmic plots of J_{sc} *versus* P_{light} (Fig. 3f), a larger α values of 0.99 is obtained for the SM-OSCs made with MDJ:Y6, indicating less bimolecular recombination.

The charge carrier mobility of the blend films was investigated using the space charge limited current (SCLC) in Fig. S11 (Supporting information). The hole mobilities (μ_h) and electron mobilities (μ_e) of the blend films were measured with hole-only device with the structure of ITO/PEDOT: PSS/active layer/MnO_3/Al and electron-only device with the structure of ITO/Al/active layer/PDINO/Al respectively. The measured μ_h and μ_e of the MDJ:Y6 and MDJ-Cl:Y6 blends are determined to $1.76 \times 10^{-4}/4.37 \times 10^{-4}$ and $0.46 \times 10^{-4}/2.79 \times 10^{-4}$ cm^2 V^{-1} s^{-1}, respectively. The hole and electron mobilities of MDJ-based blends are significantly higher than that of MDJ-Cl. The device of MDJ:Y6 has a more balanced carrier transport, thus a smaller possibility of charge accumulation and recombination. Therefore, the higher and more balanced carrier mobilities of the blend film result in higher J_{sc} and FF for MDJ:Y6 device.

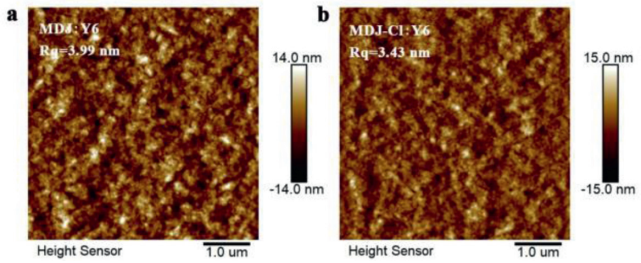

Fig. 4. AFM images of the blend films.

Miscibility between donor and acceptor materials plays a vital role in determining the morphology of the active layer. To further study the intermolecular interaction of the two donors with the acceptor, the surface tension and interfacial tension between the different donors and the acceptor Y6 were evaluated by contact angle measurements. As shown in Fig. S12 (Supporting information), the contact angle measurements of water and glycerol liquid droplets were implemented on thin films of pure materials. The surface tension of each material were quantified in accordance with the method reported in the literature [45]. The Flory-Huggins interaction factor (χ) represents the compatibility. χ can be estimated by the empirical formula $\chi = K(\sqrt{\gamma_D} - \sqrt{\gamma_A})^2$, where K is a constant and γ_D and γ_A are the surface energies of the pure films of the donor and acceptor materials, respectively. As shown in Table S2 (Supporting information), $(\sqrt{\gamma_D} - \sqrt{\gamma_A})^2$ increases significantly from 0.1149 of the MDJ-Cl:Y6 to 0.3048 (MDJ:Y6), indicating that the phase separation in the MDJ:Y6 blend is stronger. These results correspond well with that of AFM images. As shown in Fig. 4, more obvious phase separation and larger root mean square roughness (Rq) can be found in the blend of MDJ:Y6.

In summary, two novel small molecular donors were designed and synthesized. Compared with MDJ-Cl, MDJ shows a red shifted absorption spectrum, decreased miscibility with Y6, improved aggregation, suppressed charge recombination, and more efficient exciton dissociation and charge collection in the blend films. All these factors contributed to the significantly enhanced photovoltaic performance with a superior PCE of 11.16% for the MDJ-based device. Our results indicate that the SM-OSCs have a bright future for application and commercialization and highlight the significance of fine-tune the molecular structure.

Declaration of competing interest

The authors declare that they have no known competing financial interests or personal relationships that could have appeared to influence the work reported in this paper.

Acknowledgments

This work was supported by the National Natural Science Foundation of China (NSFC, Nos. 51973169, 51703172), the Open Project Program of Wuhan National Laboratory for Optoelectronics (No. 2020WNLOKF015), and the Science Foundation of Wuhan Institute of Technology (No. K202025).

Supplementary materials

Supplementary material associated with this article can be found, in the online version, at doi:10.1016/j.cclet.2021.12.055.

References

[1] P. Cheng, G. Li, X. Zhan, Y. Yang, Nat. Photonics 12 (2018) 131–142.
[2] B. Fan, X. Du, F. Liu, et al., Nat. Energy 3 (2018) 1051–1058.
[3] J. Freudenberg, D. Jansch, F. Hinkel, U.H.F. Bunz, Chem. Rev. 118 (2018) 5598–5689.
[4] X. Gao, T. Zhan, X. Zhang, et al., Nano Sel. 3 (2022) 91–97.
[5] J. Hou, O. Inganas, R.H. Friend, F. Gao, Nat. Mater. 17 (2018) 119–128.
[6] O. Inganas, Adv. Mater. 30 (2018) 1800388.
[7] Z. Liu, L. Zhang, M. Shao, et al., ACS Appl. Mater. Interfaces 10 (2018) 762–768.
[8] Z. Liu, X. Zhang, P. Ren, et al., Sol. Energy 183 (2019) 463–468.
[9] D. Deng, Y. Zhang, J. Zhang, et al., Nat. Commun. 7 (2016) 13740.
[10] K. Gao, S.B. Jo, X. Shi, et al., Adv. Mater. 31 (2019) 1807842.
[11] M. Li, K. Gao, X. Wan, et al., Nat. Photonics 11 (2016) 85–90.
[12] M. Li, F. Liu, X. Wan, et al., Adv. Mater. 27 (2015) 6296–6302.
[13] Y. Cui, H. Yao, J. Zhang, et al., Adv. Mater. 32 (2020) 1908205.
[14] L. Nian, Y. Kan, K. Gao, et al., Joule 4 (2020) 2223–2236.
[15] J. Xiong, J. Xu, Y. Jiang, et al., Sci. Bull. 65 (2020) 1792–1795.
[16] J. Min, Y.N. Luponosov, N. Gasparini, et al., Adv. Energy Mater. 5 (2015) 1500386.
[17] H. Tang, H. Chen, C. Yan, et al., Adv. Energy Mater. 10 (2020) 2001076.
[18] C. An, Y. Qin, T. Zhang, et al., J. Mater. Chem. A 9 (2021) 13653–13660.
[19] Z. Chen, W. Song, K. Yu, et al., Joule 5 (2021) 2395–2407.
[20] W. Su, Y. Wang, Z. Yin, et al., ChemSusChem 14 (2021) 3535–3543.
[21] X. Wang, D. Huang, J. Han, et al., ACS Appl. Mater. Interfaces 13 (2021) 11108–11116.
[22] J. Zhao, X. Yu, M. Zhu, et al., ACS Appl. Energy Mater. 4 (2021) 5868–5876.
[23] R. Zhou, Z. Jiang, C. Yang, et al., Nat. Commun. 10 (2019) 5393.
[24] S. Furukawa, T. Yasuda, J. Mater. Chem. A 7 (2019) 14806–14815.
[25] G.P. Kini, S.J. Jeon, D.K. Moon, Adv. Mater. 32 (2020) 1906175.
[26] H. Sun, T. Liu, J. Yu, et al., Energy Environ. Sci. 12 (2019) 3328–3337.
[27] J. Gao, J. Ge, R. Peng, et al., J. Mater. Chem. A 8 (2020) 7405–7411.
[28] H. Chen, D. Hu, Q. Yang, et al., Joule 3 (2019) 3034–3047.
[29] R. Zhou, Z. Jiang, Y. Shi, et al., Adv. Funct. Mater. 30 (2020) 2005426.
[30] J. Qin, C. An, J. Zhang, et al., Sci. China Mater. 63 (2020) 1142–1150.
[31] B. Qiu, Z. Chen, S. Qin, et al., Adv. Mater. 32 (2020) 1908373.
[32] T. Wang, L. Han, H. Wei, et al., J. Mater. Chem. A 4 (2016) 8784–8792.
[33] A. Tang, W. Song, B. Xiao, et al., Chem. Mater. 31 (2019) 3941–3947.
[34] A. Tang, Q. Zhang, M. Du, et al., Macromolrcular 52 (2019) 6227–6233.
[35] J. Zhou, P. Cong, L. Chen, et al., J. Energy Chem. 62 (2021) 532–537.
[36] J.-.N. Li, M. Cui, J. Dong, et al., Dyes Pigments 188 (2021) 109162.
[37] Y. Wang, B. Liu, C.W. Koh, et al., Adv. Energy Mater. 9 (2019) 1803976.
[38] J. Yuan, Y. Zhang, L. Zhou, et al., Joule 3 (2019) 1140–1151.
[39] K. Yu, W. Song, Y. Li, et al., Small Struct. 11 (2021) 2100099.
[40] Y. Xie, W. Wang, W. Huang, et al., Energy Environ. Sci. 12 (2019) 3556–3566.
[41] L.J.A. Koster, E.C.P. Smits, V.D. Mihailetchi, P.W.M. Blom, Phys. Rev. B 72 (2005) 085205.
[42] V.D. Mihailetchi, L.J. Koster, J.C. Hummelen, P.W.M. Blom, Phys. Rev. Lett. 93 (2004) 216601.
[43] P.W.M. Blom, V.D. Mihailetchi, L.J.A. Koster, D.E. Markov, Adv. Mater. 19 (2007) 1551–1566.
[44] S.R. Cowan, A. Roy, A.J. Heeger, Phys. Rev. B 82 (2010) 245207.
[45] Z. Zhang, H. Wang, J. Yu, et al., Chem. Mater. 32 (2020) 1297–1307.